

# Spatiotemporal investigation of the temperature and structure of a Pt/CeO<sub>2</sub> oxidation catalyst for CO and hydrocarbon oxidation during pulse activation

*Florian Maurer<sup>†</sup>, Andreas Gänzler<sup>†</sup>, Patrick Lott<sup>†</sup>, Benjamin Betz<sup>§</sup>, Martin Votsmeier<sup>§</sup>, Stéphane Loridant<sup>#</sup>, Philippe Vernoux<sup>#</sup>, Vadim Murzin<sup>§,‡</sup>, Benjamin Bornmann<sup>‡</sup>, Ronald Frahm<sup>‡</sup>, Olaf Deutschmann<sup>†</sup>, Maria Casapu<sup>†\*</sup>, Jan-Dierk Grunwaldt<sup>†\*</sup>*

<sup>†</sup> Institute for Chemical Technology and Polymer Chemistry (ITCP), Karlsruhe Institute of Technology (KIT), Engesserstraße 20, 76131 Karlsruhe, Germany

<sup>§</sup> Umicore AG & Co. KG, Rodenbacher Chaussee 4, 63457 Hanau, Germany

<sup>#</sup> Univ Lyon, Université Claude Bernard Lyon 1, CNRS, IRCELYON, F-69626, Villeurbanne, France

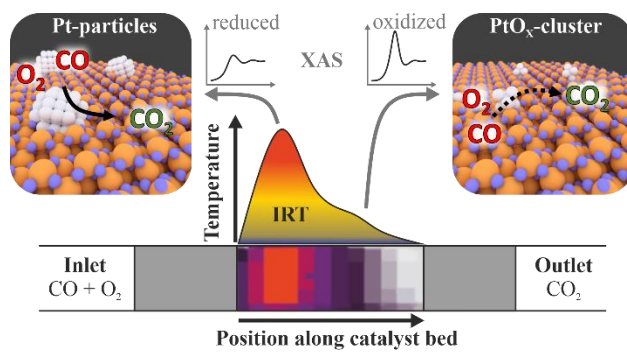
<sup>§</sup> Deutsches Elektronen-Synchrotron (DESY), Notkestrasse 85, 22607 Hamburg, Germany

<sup>‡</sup> Faculty 4 – Physics, Bergische Universität Wuppertal, 42097 Wuppertal, Germany

\*[maria.casapu@kit.edu](mailto:maria.casapu@kit.edu), \*[grunwaldt@kit.edu](mailto:grunwaldt@kit.edu)

KEYWORDS: spatiotemporal spectroscopy; spatial gas phase profiling; ceria; platinum; oxidation catalysis

## Graphical Abstract



## Abstract

Reductive treatments with pulses of CO-rich atmosphere have been used to increase and maintain the low temperature activity of a Pt/CeO<sub>2</sub>-based oxidation catalyst. A combination of *operando* infrared thermography and spatiotemporal-resolved QEXAFS on a fixed bed micro reactor unraveled that apart from the pulse length, the reaction atmosphere and the reactor temperature also the emerging reaction heat during such activating pulses have a strong influence on the structure and catalytic performance of CO and propylene conversion in axial direction of a fixed-bed and a monolithic reactor. The reductive pulse activation led to an increase of the integral catalyst activity as well as to the generation of zones of different particle sizes along the catalyst bed. In case of an activation temperature between 250 and 350 °C and pulse lengths between 5 and 30 s, a hotspot of more than 80 K was observed at the beginning of the catalyst bed. Spatially resolved X-ray absorption spectroscopy (XAS) indicate that larger and more reduced Pt particles are formed particularly at the beginning of the catalyst bed, whereas its subsequent part is less affected. Both, the length of the reductive pulses and activation temperature, have a distinct influence on the noble metal particle size. On basis of these results, a Pt/CeO<sub>2</sub> based honeycomb shaped substrate was activated in a similar manner. Spatially resolved gas phase profiling showed different reaction rates at the beginning of the reactor, which indicates that the concept can be transferred also to industrially relevant catalysts. In future, such an activation procedure might open up the door to a new class of operation strategies, where individual zones generated in the catalyst bed could be assigned for removal of specific pollutants in the exhaust stream.

## 1. Introduction

Noble metal dispersion and homogeneity are key parameters for adjusting the catalytic performance of supported metal catalysts.<sup>1-3</sup> Controlling these properties is particularly attractive for emission control catalysts since it can markedly reduce the costs of emission control systems for nearly one hundred million vehicles annually.<sup>4</sup> The microscopic structure of such catalysts is highly dynamic<sup>5</sup> and the initial activity can rapidly diminish due to aging effects like sintering,<sup>6,7</sup> incorporation into the support, oxidation or redispersion in case of Pt, which all depend on the working lean (oxygen excess) or rich (fuel excess) conditions.<sup>8,9</sup> Recently, pre-treatments involving exposure to oxidizing atmosphere at high temperature followed by reductive pulses were shown to recover or considerably increase the critical low temperature oxidation activity of Pt/CeO<sub>2</sub>-based catalysts.<sup>10,11</sup> The concept proposed by Gänzler *et al.*<sup>12,13</sup> using reductive gas pulses after a lean treatment allows to tune the noble metal particle dimensions to an optimal size for CO oxidation. This approach is highly important and needs closer examination as more recent studies demonstrated that different reactions require different noble metal particle/cluster size and oxidation state for reaching an optimal activity.<sup>7,11,14</sup> For instance, small, reduced Pt particles are efficient for CO oxidation, whereas NO oxidation is promoted by slightly larger Pt particles.<sup>7,15</sup> In both cases single site catalysts, as e.g. reported for water gas shift reaction,<sup>16,17</sup> are less effective than catalysts that contain larger Pt entities.<sup>18,19</sup>

Nevertheless, catalyst activation by application of rich periods is challenging. The approach leads to lower emissions on the long run but a pollutant-slip during the activation and, in general, the penalty due to increased fuel consumption needs to be considered as well. The integration of such a step into an already existing engine operation mode could be a possible solution for extending the catalyst lifetime. To a certain extent, lean-burn engines have such periodical treatment steps, as for instance during the regeneration of the diesel particle filter (DPF), where high temperatures are generated by adding fuel to the lean exhaust gas stream.<sup>20</sup> Another typical application using short reductive pulses are NO<sub>x</sub>-storage reduction catalysts (NSC).<sup>21,22</sup> Betz recently demonstrated a two phase activation scheme where a Pt/ceria catalyst was first activated by long reductive pulses such as used today for sulfur removal.<sup>23,24</sup> The purpose of this first long reduction was to bring the platinum in a metallic state with sufficient particle size. Such a pre-activated catalyst could then be further activated by short ~5s rich pulses, as normally used for the regeneration of NO<sub>x</sub> storage catalysts. CO light-off temperatures below 80°C were achieved in this way and a drastic

reduction of CO and HC emission during standard drive cycles was demonstrated, with negligible CO- and HC emissions due to the reductive pulses. To successfully implement such rich pulse activation sequences, the effect of certain treatment steps has to be better understood as it depends on several factors: Firstly, the pulse length and activation temperature are critical parameters that directly influence the catalyst structure, in particular the degree of reduction of the Pt-species, and thus the resulting activity. Secondly, in real-world catalytic systems, rich pulses will be more complex and might contain a substantial amount of oxygen.<sup>25</sup> In particular, exothermic processes like the reaction of oxygen with high levels of reductants will lead to a temperature increase in the catalyst bed and strong concentration gradients. Moreover, a non-homogenous reaction heat distribution due to concentration gradients and heat dissipation effects could lead to the formation of hotspots along the catalyst bed, which influence the structure of the catalyst and resulting activity along the axial direction of the catalyst bed.<sup>26–29</sup>

Such temperature gradients pose challenges but also unique opportunities for tuning the catalyst structure.<sup>30</sup> Following temperature, structure and activity gradients along the catalyst bed is thus essential and demands spatially and time resolved characterization.<sup>31–33</sup> Scale-bridging relations between hotspots on a millimeter scale and restructuring of the active phase on a nanometer scale were already reported for catalytic partial oxidation of methane over Rh/Al<sub>2</sub>O<sub>3</sub>,<sup>34,35</sup> Pd/Al<sub>2</sub>O<sub>3</sub><sup>36</sup> and CO oxidation under transient conditions, revealing valuable mechanistic insights as recently shown for Pt/Al<sub>2</sub>O<sub>3</sub> based systems.<sup>37</sup> Urakawa et al. furthermore investigated a NSC under transient conditions.<sup>38</sup> Recently, we were able to resolve different oxidation mechanisms on Pt/Al<sub>2</sub>O<sub>3</sub> and Pt/CeO<sub>2</sub> catalysts by correlating X-ray absorption spectroscopy (XAS) for a fixed bed micro reactor with spatially resolved gas phase profiling – the so-called SpaciPro technique<sup>39</sup> – along a coated honeycomb substrate.<sup>40</sup> Similarly Nagai *et al.*<sup>41</sup> investigated NSC-catalysts.

In this study, we extend the addressed complexity related to the processes occurring during catalyst activation by simultaneous spatiotemporal infrared-thermography and Quick Scanning Extended X-ray Absorption Fine Structure (QEXAFS) spectroscopy measurements on a fixed-bed micro reactor. This approach allows us to systematically investigate the evolution of hotspots emerging due to local CO-conversion and structural changes along the axial direction of the catalyst bed as function of activation temperature and pulse duration. In addition, we measure spatially resolved concentration profiles along a monolithic Pt/CeO<sub>2</sub> catalyst, to assess how the knowledge gained on the fixed-bed reactor can be transferred to honeycomb substrates including the zone-activation.

## 2. Materials and Methods

### 2.1 Materials and basic characterization

A multi-step impregnation was conducted to prepare Pt/CeO<sub>2</sub>/Al<sub>2</sub>O<sub>3</sub>.  $\gamma$ -Al<sub>2</sub>O<sub>3</sub> (Puralox, SASOL) was impregnated with an aqueous tetraammineplatinum(II) nitrate (STREM Chemicals) solution and dried under reduced pressure for 20 min at 70 °C. This step was repeated three more times until the desired platinum weight loading was achieved. The resulting powder was analogously impregnated with ceric ammonium nitrate and calcined at 500 °C for 5 h in static air. Inductively coupled plasma optical emission spectrometry (ICP-OES; 2 runs) determined a weight loading of 1.2 wt.% Pt and 4.6 wt.% CeO<sub>2</sub> on the catalyst. For the 1 wt.% Pt/CeO<sub>2</sub> sample, the same procedure was performed starting with commercial CeO<sub>2</sub>. The specific surface area was determined via N<sub>2</sub>-physisorption (BELSORP-mini II, Rubotherm) and was 28 m<sup>2</sup>/g for Pt/CeO<sub>2</sub> and 157 m<sup>2</sup>/g for Pt/CeO<sub>2</sub>/Al<sub>2</sub>O<sub>3</sub>. A monolithic catalyst sample was prepared for the spatial profiling. For this purpose, a slurry of 1.0 wt.% Pt/CeO<sub>2</sub> powder was coated on a cordierite substrate (Corning, cell density: 400 cpsi, 19 mm × 30 mm) using the dip-coating procedure. The same method for obtaining a rather homogeneous catalyst layer across the multiple channels of the cordierite monolith has been recently reported by Becher *et al.*<sup>42</sup> in an X-ray tomography study.

High-angle annular dark-field imaging-STEM measurements were performed using a Cs aberration corrected FEI-Titan (80-300 kV) and XRD using a Bruker D8 Advance ( $\lambda=0.154$  nm; 20°-90°; step size 0.015°; dwell time 2 s).

### 2.2 Combined *in situ/operando* infrared thermography and X-ray absorption spectroscopy

Combined infrared thermography (IRT) and X-ray absorption spectroscopy (XAS) investigations were performed at the P64 beamline<sup>43</sup> at DESY (Hamburg, Germany). The experiments were conducted in a quartz capillary micro reactor with plug-flow geometry, used as *in situ* cell and heated by a hot air gas blower (FMB Oxford). In order to minimize external and internal mass transport limitations, a sieved catalyst powder (100-200  $\mu$ m) was used in the fixed-bed (placed between two quartz wool plugs), that gives the best compromise between spectroscopic studies and real-world converters.<sup>44,45</sup> Gases were dosed by mass flow controllers (Bronkhorst). A mass spectrometer (Omnistar, Pfeiffer Vacuum) and FTIR (MultiGas 2030 FTIR Continuous Gas Analyzer, MKS Instruments) were used to monitor and quantify gas concentrations at the reactor

outlet on-line (Figure 1a). A weight hourly space velocity of  $60,000 \text{ L g}_{\text{Pt}}^{-1} \text{ h}^{-1}$  (GHSV:  $\sim 500,000 \text{ h}^{-1}$  at standard conditions) was used throughout all catalytic measurements.

For the tests, the capillary micro reactor (2.00 mm outer diameter, 0.01 mm wall thickness) was loaded with 13 mg of the granulated (100-200  $\mu\text{m}$ ) Pt/CeO<sub>2</sub>/Al<sub>2</sub>O<sub>3</sub> catalyst sample. CO and C<sub>3</sub>H<sub>6</sub> conversion were measured in a lean reaction mixture (1000 ppm CO, 500 ppm C<sub>3</sub>H<sub>6</sub>, 1% H<sub>2</sub>O and 8% O<sub>2</sub> in He) and under transient conditions from room temperature to 500 °C with a heating rate of 10 K/min (Figure 1c). After each light-off, the sample was held for 1 h at 500 °C under lean conditions to finely disperse Pt again.<sup>12</sup> The catalyst activation was performed consecutively using 10 reductive 5 s or 30 s pulses (3% CO, 1% H<sub>2</sub>O and 1% O<sub>2</sub> in He) with 90 s lean conditions between each pulse. The parameters for the catalyst activation were evaluated on the basis of three experiments using pulse lengths of 5 s and 30 s as well as activation temperatures of 250 °C and 350 °C. During the activation step, time resolved X-ray absorption near edge structure (XANES) spectra at the mid position of the catalyst and spatiotemporal IRT (Figure 1b) were conducted as well as spatially resolved extended X-ray absorption fine structure (EXAFS) spectra of the activated state and time-resolved XANES spectra during the light-off (Figure 1d).

Quick scanning extended X-ray absorption fine structure (QEXAFS) spectroscopy was used to collect spectra with a frequency of 1-10 Hz, resulting in 2-20 spectra per second in order to track the electronic properties of Pt during the rapid gas phase changes and transient light-off experiments. The polychromatic X-ray beam from the tapered undulator was tuned to the Pt L<sub>3</sub> edge by a liquid nitrogen cooled Si(111) channel-cut crystal as monochromator.<sup>43</sup> Special gridded ion chambers<sup>46</sup> were used to optimize the rise time for the fast measurements. With a beam size of 0.5 mm (horizontal) x 1.0 mm (vertical), 5 points along the catalyst bed were selected. For the spatially resolved EXAFS evaluation, spectra were collected for at least 5 minutes at room temperature and averaged to improve the signal quality. Pt foil and pelletized PtO<sub>2</sub> served as reference samples.

An infrared thermography camera (ImageIR 8300, Infratec; 20 mK temperature resolution) with a 25 mm lens resulting in a resolution on the sample of approx. 9 pixel/mm<sup>2</sup> and a frame rate of 80 Hz was used to monitor the hotspot formation inside the reactor during the pre-treatment (Figure 1b). The used quartz micro reactor compared to a sapphire one is a compromise for both X-ray and IRT techniques as the thin quartz wall allows simultaneous transmission of X-rays and infrared radiation for relative temperature measurements via IRT.<sup>28</sup> The calibration of the camera

was adjusted to the temperature of the pre-treatment (Calibration: “175-400 °C” for the activation at 250 °C and “300-600 °C” for the activation at 350 °C).

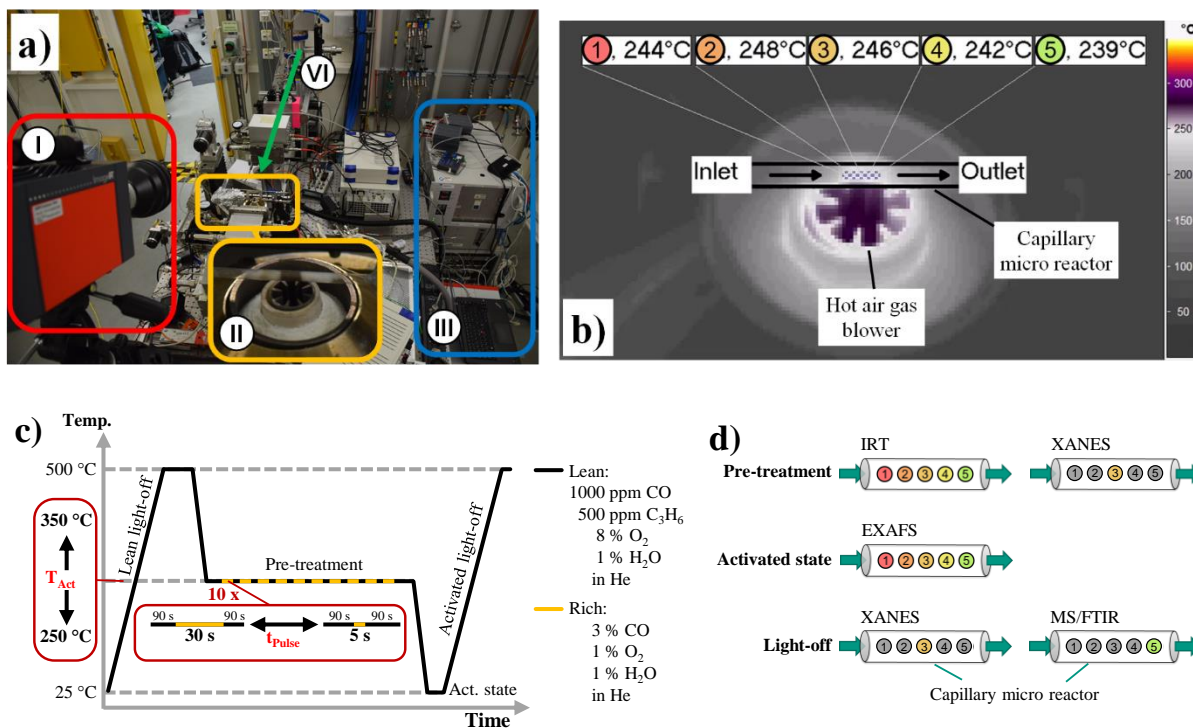


**Figure 1.** Experimental setup and sequence for the *in situ* and *operando* tests to evaluate the structure (XAS, QEXAFS), the local activity by temperature profiles and the overall catalytic activity by mass and infrared spectroscopy. (a) Experimental setup with infrared thermography camera (I), fixed-bed micro reactor and hot air gas blower system (II), gas dosage system, mass spectrometer and FTIR spectrometer (III). The trajectory of the X-rays is indicated by a green arrow (IV). (b) Snapshot of the reactor using the infrared thermography camera showing the analysis regions. (c) Overview on the catalyst test sequence and conditions with a reference lean light-off step (10 K/min in 1000 ppm CO, 500 ppm C<sub>3</sub>H<sub>6</sub>, 1% H<sub>2</sub>O and 8% O<sub>2</sub> in He), a catalyst activation with 10 reductive pulses (3% CO, 1% H<sub>2</sub>O and 1% O<sub>2</sub> in He) and a second light-off of the activated catalyst. The pulse length and the activation temperature were varied as follows: 30 s pulses at 250 °C, 5 s pulses at 250 °C and 5 s pulses at 350 °C. d: Overview on the applied characterization techniques and whether they were used spatially resolved.

### 2.3 Data evaluation

For the XAS analysis, the QEXAFS data were read-in, split and energy calibrated using the *JAQ Analyzes QEXAFS* software (version 3.3.49v5.4).<sup>47</sup> For EXAFS data, the data of 5 minutes recording was averaged and further evaluation was performed using the Demeter software package (version 0.9.21).<sup>48</sup> After normalization, background reduction and Fourier transformation (k-range



from 3.0-9.0 Å<sup>-1</sup>), the EXAFS data was fitted using structural models based on bulk Pt (ICSD 41525) and bulk PtO<sub>2</sub> (ICSD 4415) and refined using the ARTEMIS software.<sup>48</sup> Two single scattering paths for Pt-Pt (from bulk Pt; interatomic distance=2.807 Å) and Pt-O (from bulk PtO<sub>2</sub>, interatomic distance=2.070 Å) were considered for the fit, which was performed k<sup>1</sup>, k<sup>2</sup> and k<sup>3</sup>-weighted in R-space (1.00-3.00 Å). An amplitude reduction factor of 0.858 was determined by fitting the experimental EXAFS data for a Pt foil with a structure model based on bulk Pt and used for all fits (further details in Tables S1-S4 and Figures S6-S13 in the supporting information).

Transient XAS data was evaluated using a MATLAB script performing merging (for light-offs: 60 spectra were averaged, resulting in one spectrum every 30 s; for the pre-treatment: 4 spectra were averaged, resulting in one spectrum every 2 s), smoothing, energy calibration, normalization, background subtraction and the linear combination analysis (LCA) in a range from 11534 eV to 11634 eV. For the LCA, the as-prepared Pt/CeO<sub>2</sub>/Al<sub>2</sub>O<sub>3</sub> catalyst in oxygen and after a H<sub>2</sub> temperature programmed reduction at 400 °C were used as references. For plotting, the time resolved spectra were averaged and normalized using a python script based on Larch<sup>49</sup>. Time resolved IRT data was evaluated using the IRBIS 3 software (version IRBIS 3.1 professional<sup>50</sup>).

#### 2.4 Spatial profiling of the gas phase and monolithic tests

The monolithic substrate with about 19 mm diameter, 30 mm length and rectangular channels of approx. 1 mm hydraulic diameter was loaded with 1.5 g of the 1%Pt/CeO<sub>2</sub> catalyst powder resulting in a washcoat thickness of approx. 50 µm (cf. section 2.1) and was tested in a tubular quartz glass reactor. While for the *in situ* and *operando* X-ray absorption spectroscopic experiments, a catalyst with lower CeO<sub>2</sub> loading was used to increase the sample transmission, a 1%Pt/CeO<sub>2</sub> catalyst powder was used for deriving the reactant concentration profiles along the coated monolith channels. In our previous study<sup>12</sup>, it was demonstrated that both Pt/CeO<sub>2</sub>/Al<sub>2</sub>O<sub>3</sub> and Pt/CeO<sub>2</sub> catalysts show very similar catalytic properties and activation response and thus the trends can be directly compared. Mass flow controllers (Bronkhorst) were used to dose gases into the system (WHSV: 60,000 L g<sub>Pt</sub><sup>-1</sup> h<sup>-1</sup>, GHSV: ~100,000 h<sup>-1</sup> at standard conditions) and the effluent gas stream was analyzed using a Fourier transformed infrared spectrometer (FTIR; MultiGas 2030 FTIR Continuous Gas Analyzer, MKS Instruments). Spatially resolved concentration profiles were obtained by moving a thin quartz capillary (outer diameter: 170 µm) through a single central channel of the monolith and analyzing the aspirated gas with a mass spectrometer (HPR-20, Hiden

Analytical, SpaciPro setup<sup>39,51</sup>). Selected pre-treatments involving multiple reductive pulses (2% CO in N<sub>2</sub>; 15 s total reduction time at 250 °C and 10 s total reduction time at 350 °C) were performed prior to the catalytic measurements. The catalytic activity was assessed in a gas atmosphere containing 1000 ppm CO and 10 % O<sub>2</sub> in N<sub>2</sub>. In order to evaluate the spatial CO oxidation performance of the catalyst depending on the pre-treatment, the temperature for the tests were adjusted to ~50 % total CO conversion at the end of the catalytic monolith. For the transient CO oxidation tests, light-offs were performed after lean treatment (1 h; 10 % O<sub>2</sub>; 500 °C) and after pulse-activation (pulse length and quantity: 10x30 s; 2% CO in N<sub>2</sub>; 250 °C) with a ramp rate of 5 K/min in the temperature range of 75 °C to 250 °C.

### 3. Results and Discussion

Initially, catalytic CO oxidation tests were performed for a monolithic honeycomb coated with 1% Pt/CeO<sub>2</sub> to elucidate the impact of reductive pulses on the catalytic light-off activity. The monolithic honeycomb is depicted in Figure 2a (inset) and exhibits homogeneously distributed and highly dispersed Pt species, as characterized *via* HAADF-STEM and XRD measurements in Figure S1 in the supporting information and described previously<sup>40</sup>. After a treatment in 10% O<sub>2</sub> in N<sub>2</sub> at 500 °C for 1 h, a light-off test was conducted in a lean reaction mixture (1000 ppm CO, 10% O<sub>2</sub> in N<sub>2</sub>). The catalyst showed a T<sub>50</sub> (temperature of 50% CO conversion) of approx. 165 °C. By pre-treating the monolithic Pt/CeO<sub>2</sub> catalyst with multiple reductive pulses (denoted as activation steps in the following), its CO oxidation activity considerably increased. The results shown in Figure 2a reveal a decrease of T<sub>50</sub> by over 40 K to ~115 °C. For the activation step, 10x30 s pulses of 2% CO/ N<sub>2</sub> were used at 250 °C with 90 s lean reaction conditions in between. Such a treatment leads to the formation of reduced Pt nanoparticles<sup>24</sup> in the size range of 1-2 nm depending on the reducing gas atmosphere.<sup>12</sup> The resulting noble metal particles are more active than dispersed PtO<sub>x</sub> species and are able to activate the oxygen available at the perimeter sites between Pt-CeO<sub>2</sub> more efficiently,<sup>13</sup> in this way overcoming the CO inhibition effect that is typically observed for Pt/Al<sub>2</sub>O<sub>3</sub> at low temperatures.<sup>40</sup>

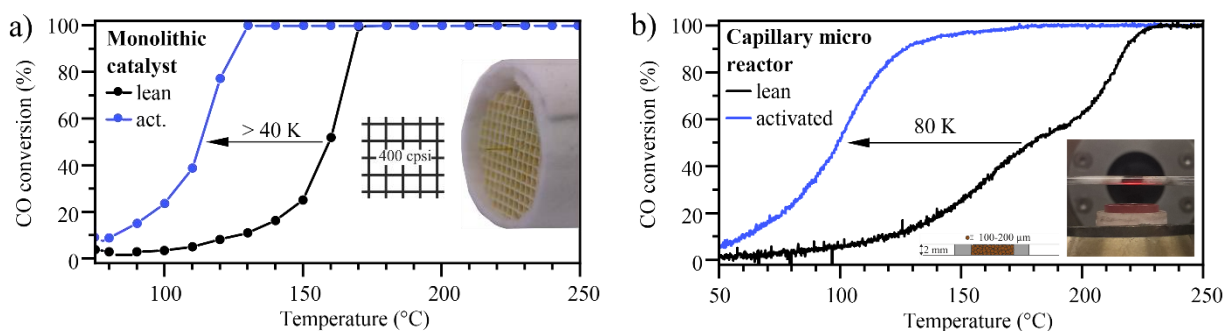


**Figure 2.** CO oxidation activity of (a) a lean and pulse activated, monolithic Pt/CeO<sub>2</sub> catalyst (cell density: 400 cpsi) and (b) a powder Pt/CeO<sub>2</sub>/Al<sub>2</sub>O<sub>3</sub> catalyst (sieve fraction: 100-200 μm). The monolithic catalyst was activated by ten 30 s pulses in 2% CO and tested in 1000 ppm CO and 10% O<sub>2</sub> (balance gas N<sub>2</sub>). For the tests in the spectroscopic quartz glass microreactor, the activation was performed using ten 30 s pulses in 2% CO and the light-off using 1000 ppm CO, 500 ppm C<sub>3</sub>H<sub>6</sub> and 8% O<sub>2</sub> (balance gas He). The same WHSV of 60,000 L g<sub>Pt</sub><sup>-1</sup> h<sup>-1</sup> was used for both tests. The activation was also found in the micro reactor for spectroscopic investigations.

As shown in Figure 2b, a similar activation effect has been observed for a Pt/CeO<sub>2</sub>/Al<sub>2</sub>O<sub>3</sub> granulated catalyst powder placed in the fixed-bed micro reactor using a quartz capillary that is suitable

for simultaneous *operando* XAS-IRT measurements. This spectroscopically accessible reactor also allows to assess the integral conversion of dosed gaseous constituents (by mass spectroscopy and FTIR) in a gas mixture containing 1000 ppm CO, 500 ppm C<sub>3</sub>H<sub>6</sub>, 1% H<sub>2</sub>O and 8% O<sub>2</sub> in He, demonstrating the ability of the micro reactor to replicate even complex reaction conditions.

However, when coupling such an activation sequence with more applied conditions, as for instance during the regeneration of a DPF in a real-world converter, the induced rich atmosphere still contains a significant amount of O<sub>2</sub>.<sup>20,25</sup> Such an environment poses new challenges on understanding the complex processes occurring like simultaneous conversion of CO, temperature increase due to the exothermic nature of oxidation reactions and hotspots formation. The role of e.g. the pulse length on the temperature along the catalyst bed was also reported by Nguyen *et al.* for the propylene oxidation over a Pt/Rh/CeO<sub>2</sub>/BaO catalyst during lean–rich cycling.<sup>52</sup> In order to elucidate their effect on the local structure along the axial direction of the catalyst bed, the effect of pulse length and temperature during activation was investigated in a spatially resolved manner using IRT, XAS/QEXAFS and overall conversion measurements. The experiments involved various gas mixtures but oxygen was present during all measurement points.

### 3.1 Effect of the pulse length

The complete test sequence for the evaluation of the influence of the pulse length is given in Figure 1c. It consisted of an initial de-greening in a lean reaction mixture step (1 h at 500 °C) followed by consecutive activation with 10x30 s pulses and 10x5 s pulses, respectively. The catalytic conversion was measured by light-offs in a lean atmosphere after the above-mentioned treatment steps. Figure 3 shows as an example the spatially and time resolved IRT images recorded during the pulse activation for the 5 s activation at 250 °C (the corresponding movie is provided as supporting information). Five positions along the catalyst bed are highlighted as representative regions for the temperature evolution inside the reactor. It can be observed that a hotspot forms during the reductive treatment stemming from high CO conversion rates and leading to an increase in temperature of up to 325 °C. The hotspot is located towards the inlet of the catalyst bed (0-4 s). When switching back to lean reaction conditions, this hotspot starts to diminish (5-9 s). While on a microscopic level, higher temperatures may occur during the pulsing, the reactor temperature can be well compared between the different pulse treatments, also because systematic errors like heat loss from the reactor are similar for all measurements. Moreover, such variations in

temperature should mainly affect the size of the noble metal particles and not induce significant gas diffusion of Pt species supported on CeO<sub>2</sub>.<sup>9</sup>

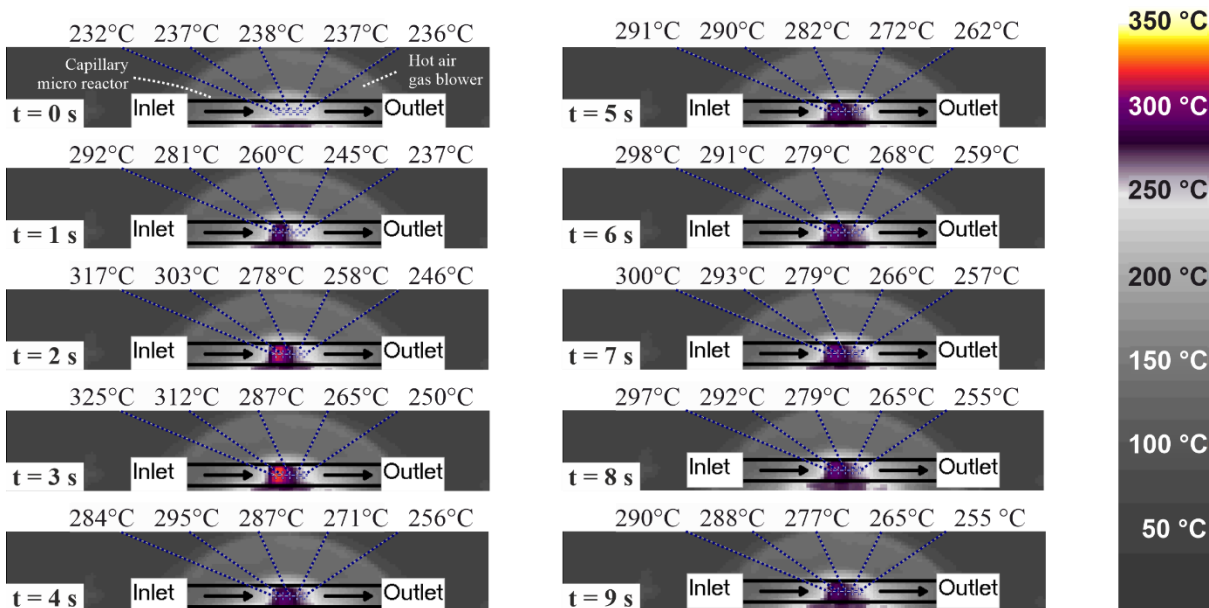


**Figure 3.** Infrared thermographic images (relative time is stated in each frame) of the capillary micro reactor during the first short reductive (CO-rich) pulse (0-4 s) of altogether 5 s at 250 °C and after switching back to lean conditions (5-9 s). The start (left) and end (right) of packed catalyst bed are indicated. Five representative positions along the catalyst bed are indicated by blue, dotted lines. The temperature is given by the color code (right) and above the infrared thermographic images for each of the five positions. The corresponding movie is supplied in the supporting information.

In order to quantify differences between the 30 s and 5 s pulses at 250 °C, time dependent data of these five regions in the catalyst bed are plotted in Figure 4c (positions along the catalyst bed from beginning to its end: red, orange, ocher, yellow, green) during the first activation pulse with 5 s and 30 s, respectively. The corresponding movies are provided as supporting information. In general, the temperature in the whole catalyst bed increased regardless of the pulse length. During the first 5 s of the reductive treatment, a hotspot located towards the beginning of the catalyst bed could be observed. The maximum temperature reached ( $T_{max}$ ) was 326 °C for the 5 s pulse and 334 °C for the 30 s pulse. Towards the end of the catalyst bed, the temperature was more than 50 K lower – irrespective of the pulse length. After 5 s, the temperature profiles changed: In the case of the short 5 s pulses, a second less dominant hotspot evolved ( $T_{max}=300$  °C), when switching back to oxidizing conditions. Interestingly, the temperature during the 30 s pulse decreased as well after approx. 5 s. This effect is particularly prevailing at the inlet of the catalyst bed, where the

temperature decreased even below the temperature observed at the end. At the 7 s mark, the temperature starts to increase again and reaches a new maximum of 340 °C. Since the oxidation of CO over Pt is highly depending on its particle size,<sup>15</sup> a possible explanation for this phenomenon could be connected to the structural evolution of Pt during the pulse. The growth of Pt particles (as uncovered by XAS, cf. later parts of the paper) together with the increase in CO and decrease of O<sub>2</sub> concentration could lead to CO poisoning of the Pt surface. Such a catalyst self-poisoning effect is well known and inhibits the catalyst bed until the CO conversion ignites again at the end of the catalyst bed once the noble metal reaches a more active state.<sup>37</sup> When switching to oxidizing conditions a second hotspot was observed, however, less dominant as seen for the short pulses.

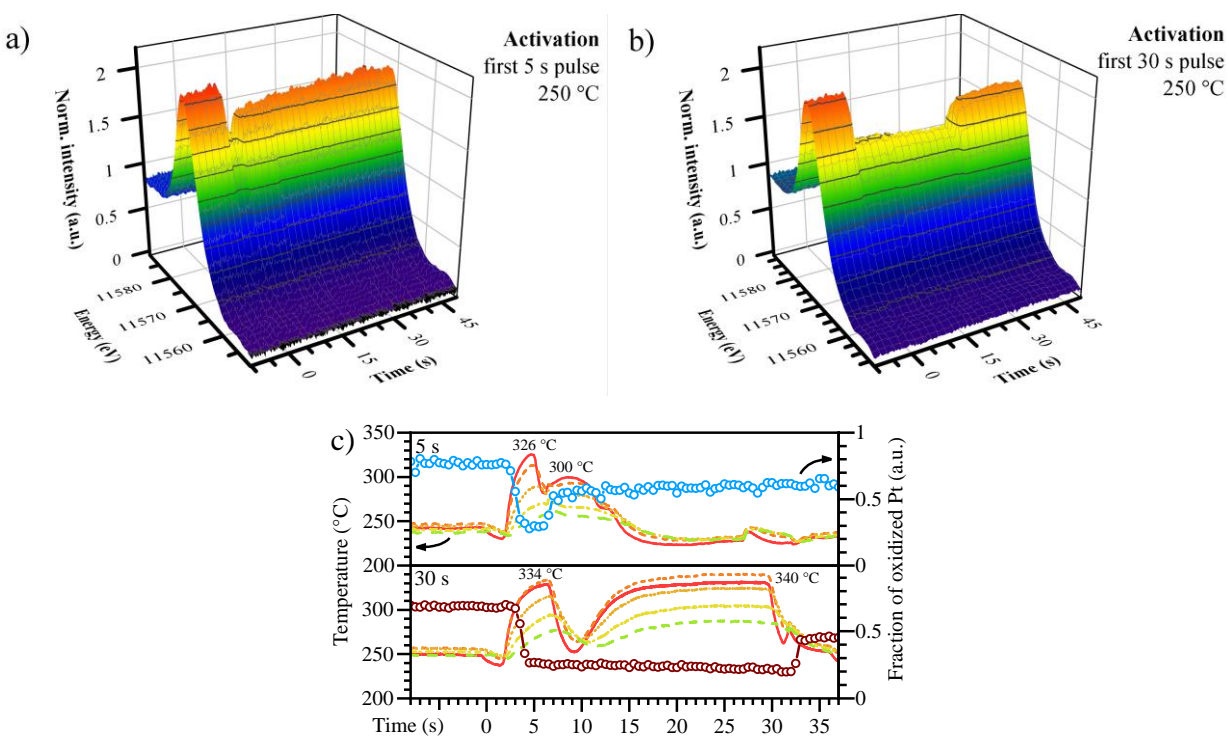


**Figure 4.** Influence of the **pulse length** on the catalyst structure and temperature evolution. QEXAFS spectra collected at the middle of the catalyst bed **(a)** during the first 5 s pulse and **(b)** 30 s pulse. **(c)** Time-dependent temperature evolution extracted from the IRT at 5 positions along the catalyst bed with its start (Pos. 1: —) more to the center (Pos. 2: ---; Pos. 3: •••; Pos. 4: -.-) and the end (Pos. 5: - -) and the oxidation state (blue and brown circles) obtained by linear combination fitting of the QEXAFS spectra in (a, b) during activation at 250 °C using 10 x 5 s (light blue) and 30 s (brown) pulses in the center of the catalyst bed (Pos. 3).

Additionally, the oxidation state of Pt during the pulses was monitored in a time resolved way in the middle of the catalyst bed during the 5 s (Figure 4a) and 30 s pulses (Figure 4b) using QEXAFS. Linear combination analysis (LCA) of these XANES data (Figure 4c, blue and brown circles) revealed, that Pt started to reduce as soon as the temperature started to rise due to the CO oxidation reaction exothermicity. This corresponds to the decrease of white-line in Figure 4a and b around the 0 s mark. When returning to lean conditions after 5 s, Pt oxidized again, but not to the same level as before the pulse, which indicates the formation of slightly larger noble metal particles.<sup>12</sup> The profile of the 30 s pulse is similar. After the initial steep decrease of the oxidation state in the first 2 s, Pt reduced continuously during the pulse. After the pulse, the noble metal oxidized markedly upon exposure to the lean mixture.

Figure 5a shows the effect of this treatment on the catalyst activity. After the treatment using ten reductive pulses of 5 and 30 s length, the catalysts are more active regarding CO and C<sub>3</sub>H<sub>6</sub> oxidation. The oxidation performance of the catalyst increased remarkably by the activation treatments, shifting the CO light-off by ~80 K from 179 °C to 93 °C and the C<sub>3</sub>H<sub>6</sub> light-off by ~50 K from 216 °C to 168 °C towards lower temperatures. Both pre-treatments led to a very similar oxidation activity of the catalyst. Figure 5b displays the XANES data collected at the center position (position 3) of the micro reactor after ten 5 s and 30 s pulses compared to the catalyst treated only under lean conditions. The lean-treated catalyst exhibits the strongest so-called white-line of the Pt L<sub>3</sub> edge with a maximum intensity at ~11569 eV indicating a high oxidation state (Figure S2 in the supporting information). This feature is significantly less dominant for the pulse-activated samples. Thus, the noble metal species remained significantly more reduced, although the catalyst was exposed to lean conditions after the CO-rich pulse. The oxidized fraction could emerge from redispersed species or surface oxidation of Pt particles. The reduction degree was only slightly higher after ten 30 s pulses with slightly lower white-line than ten 5 s pulses. The state after activation was additionally characterized by spatially resolved XANES and EXAFS measurements. The results unraveled that the oxidation state, as determined by linear combination analysis and evaluation of Pt-Pt and Pt-O coordination numbers normalized to those in bulk Pt and PtO<sub>2</sub> (exact coordination numbers, see Tables S1-S4 in the supporting information), varied significantly along the fixed bed. This is summarized in Figure 5c and demonstrates a strong dependence on the activation treatment. The spatially resolved XANES data along the reactor are depicted in Figure 5d and f. The glitch at 11555 eV appears due to defects on the monochromator

crystal. The strong gradient, indicated in particular by the coordination numbers, uncovers a strong change in the size of the particles and their oxidation state along the catalyst bed. The closer the coordination number of the Pt-Pt tends towards 12 (in Figure 5c given as relative number 1), the

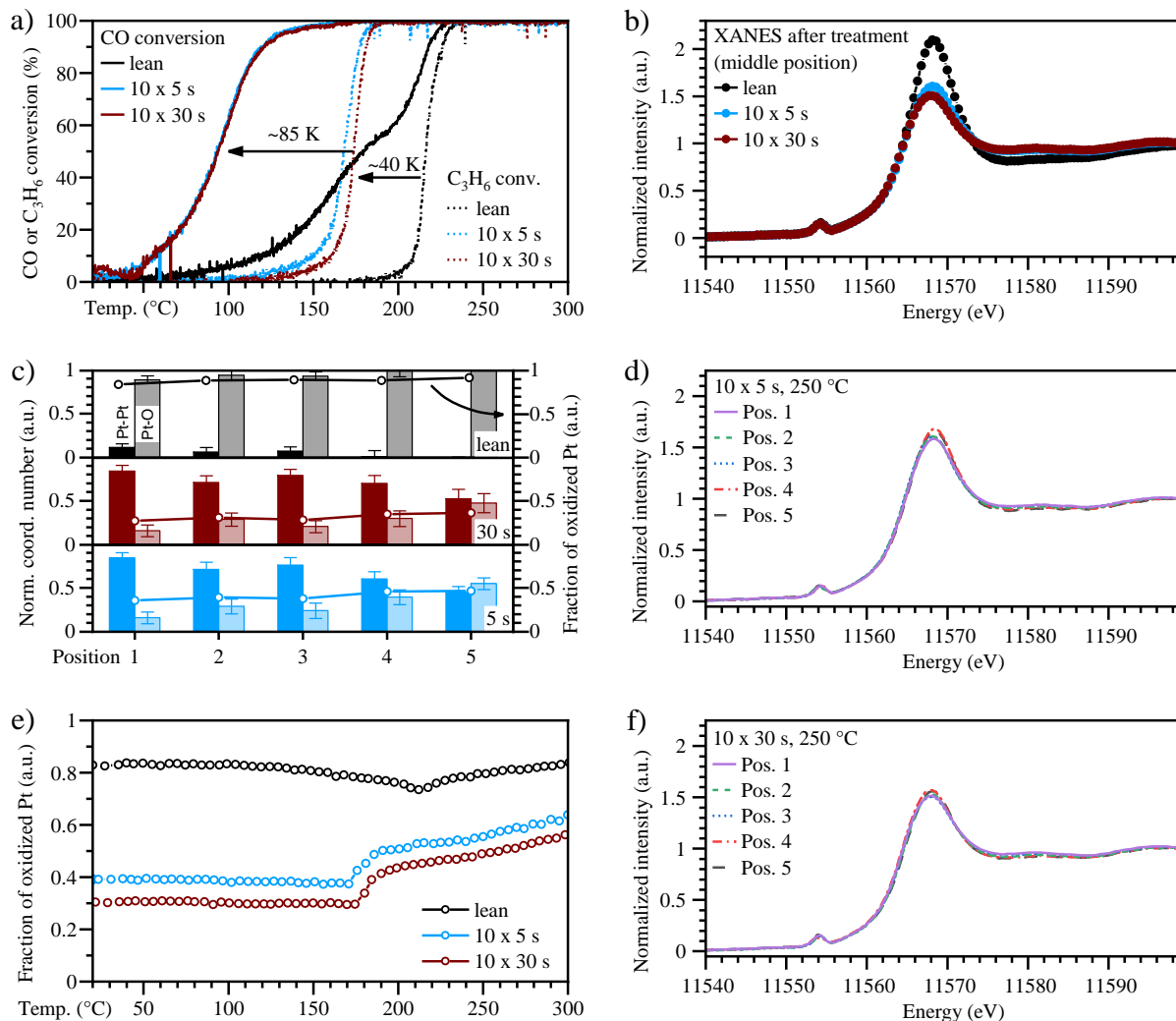


**Figure 5.** Influence of the **pulse length** on catalyst activation. **(a)** catalytic CO (solid lines) and C<sub>3</sub>H<sub>6</sub> (dotted lines) conversion during a light-off with 10 K/min in 1000 ppm CO, 500 ppm C<sub>3</sub>H<sub>6</sub>, 1% H<sub>2</sub>O and 8% O<sub>2</sub> in He. Prior to this treatment, the catalyst underwent a lean treatment (black lines) or an activation using ten 5 s pulses (light blue) or 30 s reductive pulses (brown) at 250 °C. **(b)** XANES spectra after the respective treatments. **(c)** relative coordination numbers (bars) of Pt-Pt and Pt-O coordination number obtained by EXAFS analysis together with the fraction of oxidized Pt species (circles) determined by linear combination analysis. In **(d, f)**, the corresponding XANES data are displayed. **(e)** fraction of oxidized species during the light-off derived from *operando* QEXAFS (cf. Figures S14, S15 and S17 in the supporting information) in the middle of the catalyst bed (LCA of XANES) of the two pulse-activated catalysts in comparison to the one treated under lean conditions.



larger are the Pt particles. Analogously, if the Pt-O coordination number is 6, the first coordination sphere would be completely filled by O atoms (relative number 1). Both pulse-activation treatments increased the Pt-Pt coordination numbers compared to the lean treated sample, particularly at the inlet of the catalyst bed. This trend is more distinct for the sample treated with 30 s pulses than that after the 5 s pulse activation step, indicating that larger particles were formed during the longer pulses. Strikingly, this correlates with the hotspot that occurs more at the beginning of the catalyst bed under the applied pulse-activation conditions.

*Operando* XAS data collected during the transient catalytic activity measurements (1000 ppm CO, 500 ppm C<sub>3</sub>H<sub>6</sub>, 1% H<sub>2</sub>O, 8% O<sub>2</sub> in He) are shown in Figure 5e, and uncover that the course of the oxidation state during the light-off is qualitatively very similar for the 5 s and 30 s pulse-activated samples: The middle of the catalyst bed remained reduced until most of the reductive components are converted. As soon as C<sub>3</sub>H<sub>6</sub> got converted, Pt started to oxidize. However, according to the EXAFS analysis, the treatment with 30 s pulses led to larger Pt particles and this also resulted in a lower oxidation state above the light-off temperature. This offset in oxidation state remained throughout the light-off.

As expected, a lean treatment leads to highly oxidized Pt species. The high oxidation state of these Pt entities indicates the presence of highly dispersed PtO<sub>x</sub> clusters or even cationic Pt<sup>2+</sup> single sites that have been reported to be less active than partially reduced or metallic particles/clusters.<sup>18</sup> These species are gradually reduced upon onset of CO and C<sub>3</sub>H<sub>6</sub> conversion, what can be seen in Figure 5e by a decrease of the Pt oxidation state by nearly 10% between 100 °C and 210 °C for the lean sample. Such a behavior of Pt to reduce during the light-off was already reported in previous studies.<sup>53</sup> When most of the pollutants are converted, Pt starts to oxidize again as the reductants are completely converted at the beginning of the catalyst bed.

The following conclusions can be drawn from these first measurement series: Despite differences in the particle size and oxidation state occur particularly towards the end of the catalyst bed, the 5 s and 30 s pulse-treated catalysts exhibit nearly the same CO oxidation performance. Hence, under similar reaction conditions (in terms of space velocity and gas concentrations), as applied in this study, short reductive pulses seem to be more attractive, since less fuel (in terms of CO and C<sub>3</sub>H<sub>6</sub>) would be used for the catalyst activation. This might change when going to higher temperatures around 400 °C when Pt starts to redisperse<sup>12</sup> and the pulse reduction has to be repeated in order to maintain the high activity. As smaller particles are less stable than larger

particles<sup>54</sup>, the redispersion is expected to be faster after the 5 s pulses than after the 30 s pulses. During operation of a NO<sub>x</sub>-storage catalyst, such short, periodic reductions have already been shown to be beneficial to maintain a high catalytic activity,<sup>22,55</sup> which is likely due to the stabilization of metallic Pt particles.

Due to the presence of oxygen under rich conditions, the temperature gradients formed during the pulsing sequence lead to structural variations along the fixed-bed reactor, which could be avoided by the application of more advanced reactor concepts.<sup>56</sup> Particularly, the hotspot at the catalyst inlet occurring under rich conditions seems to play a key role during the formation of larger and more active Pt particles. The maximum temperature observed under lean conditions at these points are at least 50 K lower (note that IR thermography measures the outer part of the catalyst bed). Higher temperatures and thus higher reaction rates during the activation could increase this spatial activation effect even further, leading to an improved overall activity.

### *3.2 Influence of the activation temperature*

To investigate the role of the temperature during pulse activation, the measurements were conducted both at 250 °C and 350 °C and involved short pulses of 5 s for catalyst activation along with the sequence used before (see Figure 1c). With regard to extent ( $\Delta T \sim 70$  K) and location, infrared thermography results (Figure 6a and b) showed a similar hotspot at the inlet position for both activation temperatures under reducing conditions (0-5 s). When switching back to oxidizing conditions (5-10 s), a second temperature increase was observed reaching 300 °C and 397 °C for an activation temperature of 250 °C and 350 °C, respectively. Regarding the state of the catalyst during these transient steps, the evaluation of the XANES spectra collected at the mid catalyst bed position (Position 3, Figure 6a and b) indicates that a more pronounced reduction occurs for Pt sites during the activation at 350 °C. However, due to the higher temperature and more localized conversion<sup>28</sup> at the inlet of the catalyst bed, at mid position the state of Pt after switching back to the reaction gas atmosphere and 10 s exposure is comparable for the catalyst activated at 350 °C with that treated at 250 °C.

Nevertheless, strong differences in the activated state were observed along the catalyst bed: upon the 350 °C activation, Pt exhibited a lower Pt-Pt coordination number throughout the catalyst bed according to the EXAFS fitting (Figure 6c). Together with the slightly higher oxidation state after activation, the treatment at 350 °C seemed to generate smaller and more oxidized Pt particles. In

a previous study, we investigated the redispersion of Pt using environmental transmission electron microscopy. The migration of single Pt atoms from the particles to the support CeO<sub>2</sub> was observed with temperatures starting at 400 °C.<sup>12</sup> Similar temperatures (Figure 6b, T<sub>max</sub>=397 °C) were found upon returning to lean conditions after the reductive activation pulse. Thus, exceeding this temperature threshold under lean conditions, has obviously led to the reoxidation and redispersion of Pt particles resulting in a lower coordination number for Pt-Pt neighbors.

Figure 6d shows the following light-off curves and the corresponding LCA results of the *operando* QEXAFS measurements during CO and C<sub>3</sub>H<sub>6</sub> oxidation. Using a pulse activation at 350 °C shifted the light-off curves for CO by ~14 K and for C<sub>3</sub>H<sub>6</sub> by ~10 K towards higher temperatures as compared to an activation at 250 °C. Thus, when increasing the activation temperature, the activation was less effective. The linear combination analysis of XANES during these catalytic assessments revealed further structural differences after the pulse activation at 250 °C and 350 °C. For an activation at 250 °C, the oxidation state of Pt stayed stable and remained more reduced until all reductants were oxidized. In contrast, the oxidation state in the catalyst activated at 350 °C decreased slightly (from 45% PtO<sub>2</sub> at 53 °C to 39 % PtO<sub>2</sub> at 177 °C) during the onset of CO and C<sub>3</sub>H<sub>6</sub>-oxidation. Such a behavior was also found for the lean treated catalyst, in line with our previous studies.<sup>53</sup> This indicates that Pt particles do not have the optimal size and state for CO and C<sub>3</sub>H<sub>6</sub> oxidation in both the high temperature activated samples and especially in the catalyst exposed to lean conditions. As demonstrated by the XANES data, the fraction of oxidized Pt is higher along the whole catalyst bed (Fig. 6c) for the 350 °C pulse-activated sample compared to the one treated at 250 °C. This is as well supported by the EXAFS data analysis, showing that the Pt-Pt coordination after the 350 °C treatment was lower as compared to the 250 °C activation throughout the whole catalyst bed. This is in contrast to the comparison of the 5 s and 30 s pulses, where the differences were localized at the outlet of the catalyst bed. When comparing the coordination numbers at the start of the catalyst bed, a number of 8.6 (normalized CN at position 1: 0.72) was obtained after pulsing at 350 °C in contrast to 10.1 (normalized CN at position 1: 0.84) as determined upon activation at 250 °C. However, when deducing the Pt-particle size from the Pt-Pt coordination number by using geometric models,<sup>57</sup> these rather small differences correspond to nearly a factor of 2 in particle size (~1-2 nm after 350 °C and ~2-3 nm after the 250 °C), which may have led to an overall lower catalytic activity for the sample activated at 350°. Due to the restraints of the EXAFS model (Tables S1-S4 and Figures S6, S8, S10, S12 in the

supporting information), the absolute coordination numbers determined by the applied EXAFS model may overestimate the Pt-Pt coordination number. Therefore, a second fitting model was applied (Figures S6, S8, S10, S12 in the supporting information). However, the relative trends along the catalyst bed and also between the activation temperatures remained unchanged.

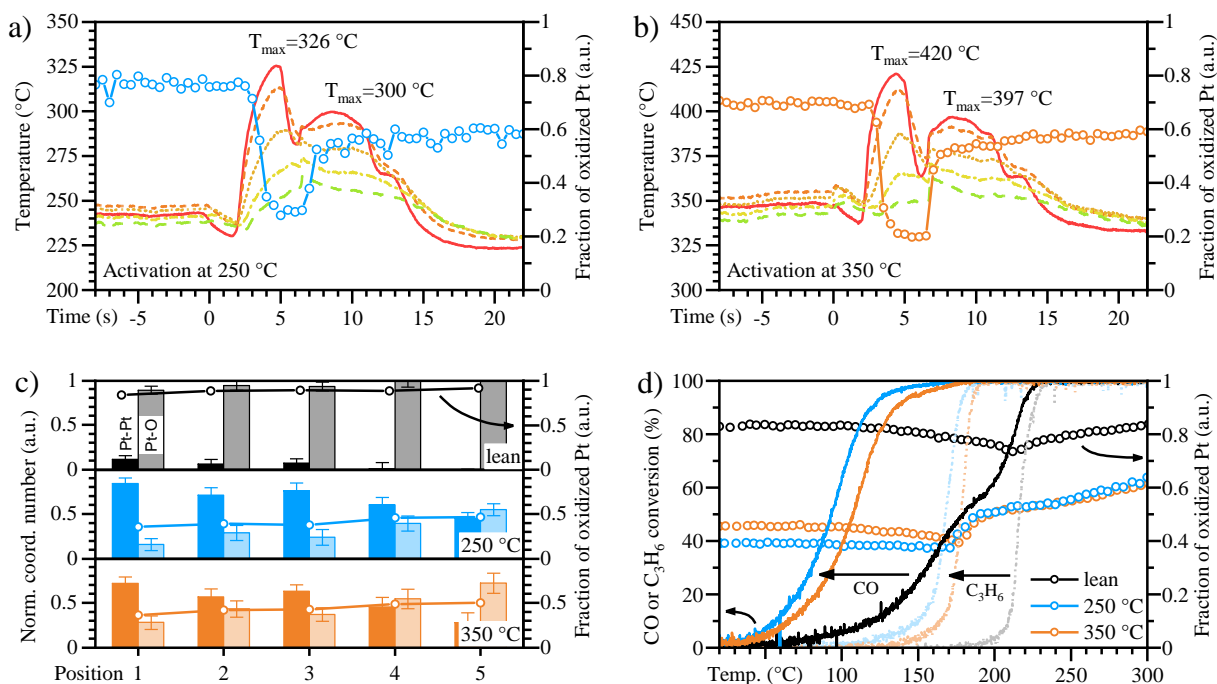


**Figure 6.** Influence of the **activation temperature** on the catalyst activation. **(a)** Time-dependent temperature evolution extracted from the IRT at 5 positions along the catalyst bed ranging from its inlet (Pos. 1: —) via the center (Pos. 2: ---; Pos. 3: ···; Pos. 4: -.-) to its end (Pos. 5: - -; see overview in Figure 1) and XANES at center position (circles) results during activation at 250 °C and **(b)** 350 °C using ten 5 s pulses; **(c)** relative coordination numbers (bars) of Pt-Pt and Pt-O obtained by EXAFS analysis and fraction of oxidized Pt (circles) from linear combination analysis, after pulse-activation at 250 °C (blue) and 350 °C (orange) using ten 5 s pulses; **(d)** catalytic CO and C<sub>3</sub>H<sub>6</sub> oxidation activity (light-off with 10 K/min in 1000 ppm CO, 500 ppm C<sub>3</sub>H<sub>6</sub>, 1% H<sub>2</sub>O and 8 % O<sub>2</sub> in He) after pulse-activation at 250 °C (blue) and 350 °C (orange) using ten 5 s pulses and corresponding oxidation state (circles, determined by LCA of XANES) monitored by *operando* QEXAFS (cf. Figures S14-S16 in the supporting information) in the middle of the catalyst bed.

All in all, for preserving an optimal electronic state of Pt on CeO<sub>2</sub> temperatures around or higher than 400 °C under oxidizing conditions should be avoided during and especially after the activation process. By deliberately exploiting the local temperature increase, i.e. hotspot formation, new possibilities arise in tuning the catalyst structure along the catalyst bed. As the pulse activation at 250 °C indicates, an accurate tuning of the activation temperature and pulse

duration can lead to individually activated zones along the catalyst bed. Since the Pt particle size with the highest oxidation activity depends on the nature of the pollutant,<sup>7,15</sup> this approach might offer new opportunities in increasing the low temperature performance of diesel oxidation catalyst.

### *3.3 Using temperature gradients to enhance the local CO oxidation activity*

In order to generalize the results and to transfer to a more realistic catalyst system, we aimed in a next step at activating a monolithic Pt/CeO<sub>2</sub> catalyst for CO oxidation considering the changes in structure along the axial direction of the catalyst bed. For this purpose, a stepwise reduction was first applied for a powder Pt/CeO<sub>2</sub>/Al<sub>2</sub>O<sub>3</sub> catalyst by variation of multiple reducing pulses in the range of 2 s to 30 s as shown in Figure 7a into an inert atmosphere (He) to monitor the reduction front through the catalyst bed. By monitoring the oxidation state after each pulse at 250 °C (Figure 7b) at five positions (see Figure 7a), the spatial structural gradients were estimated by QEXAFS as function of the pulse-activation time. To avoid redispersion between the pulses, an inert atmosphere was used while recording XAS. The influence of hotspot formation was taken into account by repeating this treatment at 350 °C (Figure 7c), which is corresponding to the maximum temperature reached during the 5 s and 30 s treatment (Figure 4c).

For both activation temperatures, no changes were observed during the 2s activation pulses (see LCA in Figure 7b). The corresponding XANES data are shown in Figure S3 in the supporting information, uncovering that the white-line and thus oxidation state stays on the level of the lean treated catalyst. Hence, the stepwise reduction at 250 °C seems to have a threshold regarding pulse length. In our previous studies, we have found that the reduction of highly dispersed Pt is energetically more difficult compared to the case where preexisting Pt-clusters or nanoparticles are on CeO<sub>2</sub> surfaces.<sup>13</sup> Furthermore, even after the formation of reduced clusters containing only a few Pt- atoms, these entities are particularly prone to re-oxidation under reaction conditions.<sup>15,18</sup> Increasing the pulse duration to 5 s leads to significant Pt reduction at 250 °C. However, this reduction seems to occur homogeneously throughout the catalyst bed. More reductive pulses ranging from 5 to 30 s lead to a further and evenly distributed oxidation state decrease along the catalyst bed. The same experiment performed at 350 °C (Figure 7c, XANES are given in Figure S4 in the supporting information) results in a different outcome. While 2 s pulses do not induce significant reduction, the first and second 5 s pulse cause structural gradients, with the beginning of the catalyst bed

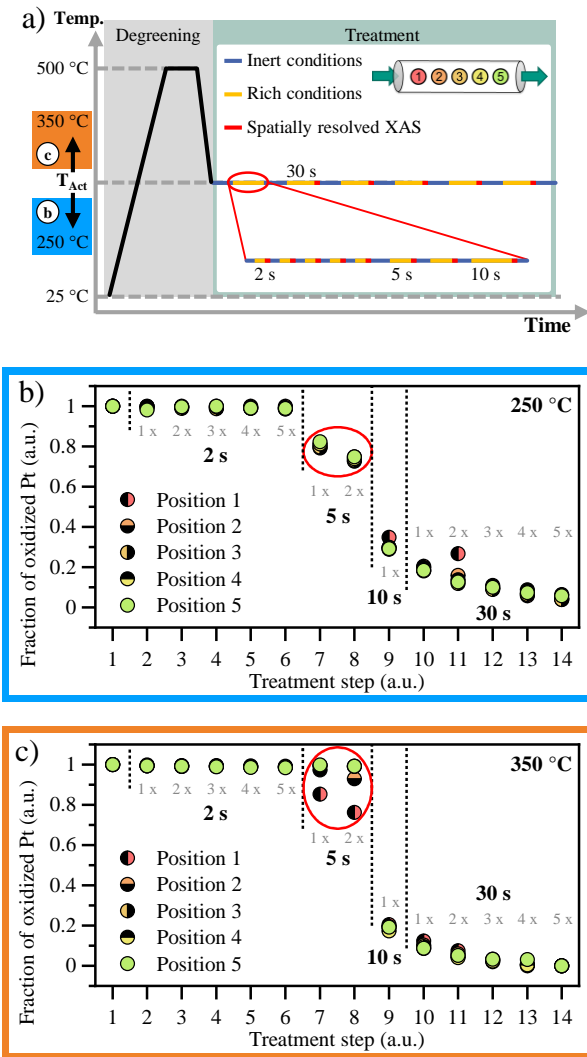


**Figure 7.** (a) Schematic sequence for the stepwise reduction of the Pt/CeO<sub>2</sub>/Al<sub>2</sub>O<sub>3</sub> catalyst; oxidation state of Pt after treatment steps with reductive pulses (2% CO in He) in an inert atmosphere (He) ranging from 2 s to 30 s at (b) 250 °C and (c) 350 °C. The fraction of oxidized species is presented spatially resolved at 5 positions along the catalyst bed ranging from its inlet (red) to the outlet (green) and estimated by LCA of the spatially resolved XANES. The spectra were normalized to the lean treated sample and after complete reduction at the respective position.

being 20% more reduced than the end. When exposed to additional and longer pulses, the Pt oxidation state gets uniform again along the catalyst bed. To evaluate the impact of a local activation at the beginning of the catalyst bed and to transfer the insights to a monolithic catalyst, spatially resolved gas phase concentration assessments were used to correlate the CO conversion with the position along a monolithic Pt/CeO<sub>2</sub> catalyst, as also applied for other heterogeneously catalyzed reactions<sup>58</sup>. In Figure 8a, the CO concentration profile is reported for the coated monolith over a 30 mm channel length after three pre-treatments: lean, pulse activation at 250 °C with multiple pulses, and an accumulated reduction length of in total 15 s and at 350 °C for in total 10 s under reductive conditions. The temperature during the spatially resolved activity measurement was set to  $T_{50}$  to keep the CO conversion at approx. 50 %.  $T_{50}$  for the lean treated sample was 128.5 °C. By pulse activation, it was successfully shifted by 29.5 K ( $T_{50}=99$  °C) and more than 31 K ( $T_{50}=97.5$  °C) for the 350 °C and 250 °C treatment, respectively.

Spatially resolved gas phase assessment revealed differences in the CO concentration profiles along the catalyst for the three pre-treatments. To increase the visibility of these

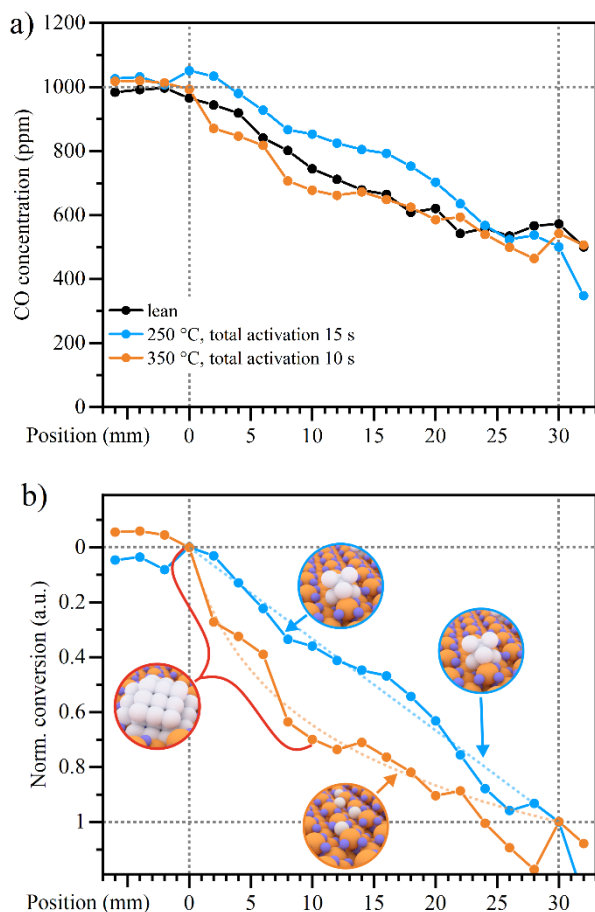


**Figure 8.** (a) CO concentration profiles in 1000 ppm CO and 10% O<sub>2</sub> in N<sub>2</sub> along a 3 cm long monolithic honeycomb substrate coated with a Pt/CeO<sub>2</sub> catalyst at a T<sub>50</sub> temperature of 128.5 °C after a lean treatment (black), at T<sub>50</sub>=97.5 °C after activation at 250 °C with an accumulated pulse length of 15 s (blue) and T<sub>50</sub>=99 °C after activation at 350 °C with an accumulated pulse length of 10 s (orange). (b) For a better visibility, the CO conversion profiles were normalized to the CO concentration at the inlet (0) and outlet of the reactor (1). Dotted lines are a guide to the eye to highlight the trends of the CO conversion. The red bracket indicates the high conversion at the beginning of the catalyst bed for the catalyst activated 350 °C. Based on the previous XAS results, the Pt particle size along the catalyst bed is schematically illustrated in the circles as inset.

differences, the CO conversion was normalized along the catalyst in Figure 8b. For this, the CO conversion at the start of the honeycomb was set to 0 and at the end to 1. The CO concentration for the sample activated at 250 °C resembled a straight line (illustrated by the blue, dotted line in Figure 8b), meaning that the same catalytic activity is reached along the whole catalyst bed. After a lean treatment and pulse activation at 350 °C, the catalyst exhibited a CO concentration profile, where more CO is converted at the inlet of the catalyst and less at the outlet (indicated by the dotted, orange line in Figure 8b). The red bracket in Figure 8b highlights the steep increase of the CO conversion at the catalyst bed inlet compared to the 250 °C sample. For the 250 °C and 350 °C activation, these differences can be explained considering the information from the XAS results (Figure 7b and c). After a pulse treatment at 250 °C, Pt entities with a highly homogeneous oxidation state and particle size along the whole catalyst were formed regardless of the pulse length. Since the same active species were present at all positions of the catalytic monolith, the same CO-conversion rate along the catalyst was achieved – resulting in a straight line in terms of CO concentration or conversion. Such a zero reaction order with respect to CO was also observed in recent studies for Pt nanoparticles

on  $\text{CeO}_2$ .<sup>40</sup> The activation at higher temperatures with one or two 5 s pulses generated reduced and larger particles nearly exclusively at the beginning of the catalyst bed (Figure 7c). Thus, a higher CO conversion rate is found particularly in this region. As seen above (cf. Figure 6c), the lean treated catalyst exhibited also structural gradients along the catalyst bed. Since at 500 °C (temperature of the lean treatment) most of the CO and  $\text{C}_3\text{H}_6$  conversion occurs at the beginning of the catalyst bed and locally prevents the redistribution of Pt particles, this zone contains more reduced Pt than the middle and end of the monolith channel. Thus, despite showing a significantly lower overall performance ( $T_{50}=128.5$  °C), the oxidized catalyst behaves similarly to the 350 °C spatially activated sample with respect to the CO concentration profile.

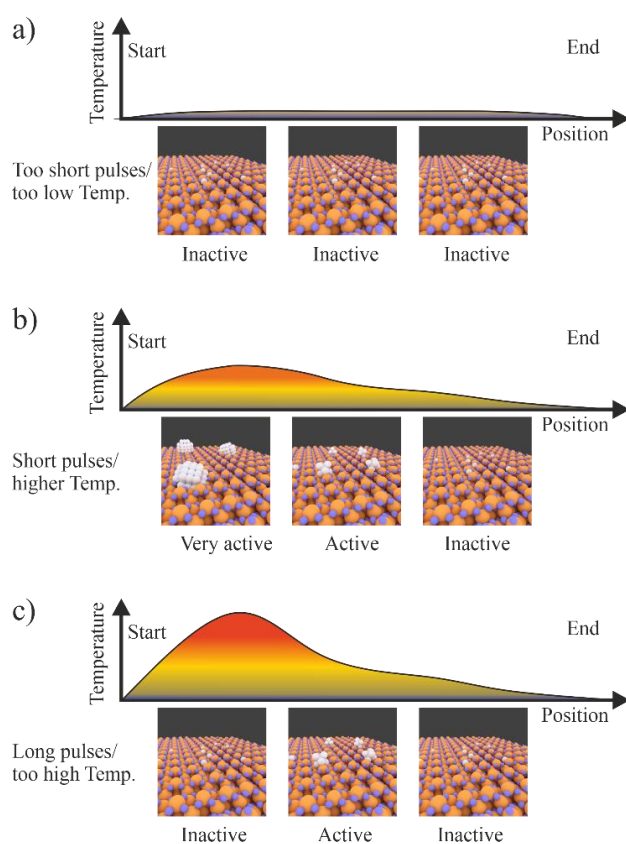


**Figure 9.** Schematic view on the hotspots and the resulting Pt-species/particles evolving during CO-rich pulses with strong consequences for CO oxidation along a monolithic catalyst, which is considered a new conceptual tool to tune the noble metal component (grey spheres) in axial direction of a fixed bed reactor/monolithic catalyst: **(a)** if the pulse length is too short or the activation temperature set too low, no particles are formed and no CO conversion is observed. **(b)** Using short reductive pulses at a higher temperature leads to the formation of hotspots, that can be used to trigger the localized formation of larger and very active Pt particles. **(c)** In case of too long pulses or a too high temperature of activation, Pt particles will directly re-disperse under the lean atmosphere cancelling out the positive effects of the activation.



A pulse activation with short pulses conducted at higher temperatures thus obviously triggered structural gradients along the catalyst bed. These gradients lead to different zones in the reactor with higher and lower activity, as exemplarily shown for CO oxidation in schematic Figure 9. These differences may be further explored in future applications for the generation of zones with varying noble metal particle size and oxidation states along a structured catalyst. Since the oxidation of emissions like CO, HC or NO is preferred on different catalytic sites, each of these zones could be optimized with respect to the conversion of a certain pollutant or for specific reaction conditions like lean/stoichiometric/rich conditions, high/low temperatures or catalyst poisons.

#### 4. Conclusion

Reductive pulse-activation treatments are a promising approach to increase and maintain the low temperature activity of Pt-based catalysts for emission control. Particularly, pulses with CO-rich atmosphere were shown to efficiently tune the activity profile of Pt/CeO<sub>2</sub> based catalysts. In this study, a novel combination of *operando* infrared thermography and spatially and time-resolved X-ray absorption spectroscopy on a fixed bed micro reactor allowed us to correlate the Pt structure and structural gradients along the catalyst bed with the integral catalytic activity. This knowledge could then be used to interpret spatial effects in a monolithic catalyst by gas phase profiling.

By adjusting the reduction parameters, we were not only able to efficiently optimize the amount of reductants and thus the fuel penalty but also observed structural changes along the reactor. Using infrared thermography, the position and extent of hotspots could be quantified. Under reducing conditions and in the presence of oxygen, the temperature particularly at the inlet of the catalyst bed increased by more than 70 K. Higher temperatures led to larger and more reduced Pt particles. However, if the catalyst activation temperature was set too high, Pt oxidized and redispersed again, leading to a state similar to the lean treated sample. On basis of these results, we were able to use this combination of reducing pulses, structural changes and emerging reaction heat due to the exothermicity of the reaction during such activating pulses to spatially activate a Pt/CeO<sub>2</sub> based monolithic catalyst for enhancing its CO oxidation activity at the inlet.

Such an *in situ* activation during operation opens up the door to a new class of operation strategies: combining the activation of an oxidation catalyst with the regeneration of a NO<sub>x</sub>-storage catalyst or the generation of individual zones in the catalyst bed to attribute for the amount and nature of the pollutants in the exhaust gas stream. The latter might be achievable by further optimization of the pulsing parameters in terms of the space velocity or reductant concentration. By this, the overall emissions of toxic pollutants may be further reduced and the critical low temperature activity enhanced.

## ASSOCIATED CONTENT

### Supporting Information

The Supporting Information is available free of charge at <https://pubs.acs.org/doi/10.1021/acs.iecr.xxxxx>

Additional catalyst characterization results (XRD, TEM of the as-prepared Pt/CeO<sub>2</sub>/Al<sub>2</sub>O<sub>3</sub> and Pt/CeO<sub>2</sub> catalysts), additional XANES and QEXAFS data, information on the EXAFS data evaluation and 3 movies on the infrared thermographic measurements during the catalyst activation (reductive CO-rich pulses followed by switching back to lean conditions) with are provided as supporting information (IRT movies with 5s pulses at 250 °C, 5s pulses at 350 °C, 30 s pulses at 250 °C).

### Data Availability Statement

All data generated or analyzed during this study are included in this published article (and its supporting information files) or can be obtained from the authors upon reasonable request.

### Corresponding Author

Correspondence should be addressed to [Maria Casapu \(maria.casapu@kit.edu\)](mailto:maria.casapu@kit.edu) and [Jan-Dierk Grunwaldt \(grunwaldt@kit.edu\)](mailto:Jan-Dierk.Grunwaldt@kit.edu).

### Author Contributions

The manuscript was written through contributions of all authors. All authors have given approval to the final version of the manuscript.

### Funding Sources

There are no competing interests.

## ACKNOWLEDGMENT

This paper is dedicated to Professor Enrico Tronconi in honor of his outstanding contributions towards a better understanding of the behavior of catalytic reactors. The authors gratefully acknowledge the German Federal Ministry for Economic Affairs and Energy (BMWi: 19U15014B) and the French National Research Agency (ANR-14-CE22-0011-02) for funding the DEUFRAKO collaboration ORCA. The DFG is thanked for financial support of infrastructure at KIT (INST 121384/16-1, INST 121384/73-1, INST 121384/73-1) and DESY for beamtime at the P64 beamline. Moreover, the work was funded by the Deutsche Forschungsgemeinschaft (DFG, German Research Foundation) – Project-ID 426888090 – SFB 1441.

D. Zengel, G. Cavusoglu and D. Doronkin (ITCP/IKFT, KIT) are appreciatively acknowledged for assistance during *operando* XAS experiments as well as J. Pesek (ITCP, KIT) and P. Dolcet (ITCP, KIT) for technical support with respect to catalyst testing and T. Bergfeldt (IAM-AWP, KIT) for ICP-OES analysis. Finally, W. Caliebe and Marcel Görlitz (P64, DESY) are thanked for support during beamtime. R. F. and V.M. are grateful for financial support from the BMBF project 05K19PXA. F.M. (ITCP, KIT) and P.L. (ITCP, KIT) thank the “Fonds der Chemischen Industrie” (FCI) for financial support during their PhD studies.

## REFERENCES

- (1) Resasco, J.; Derita, L.; Dai, S.; Chada, J. P.; Xu, M.; Yan, X.; Finzel, J.; Hanukovich, S.; Hoffman, A. S.; Graham, G. W.; Bare, S. R.; Pan, X.; Christopher, P. Uniformity Is Key in Defining Structure-Function Relationships for Atomically Dispersed Metal Catalysts: The Case of Pt/CeO<sub>2</sub>. *J. Am. Chem. Soc.* **2020**, *142* (1), 169–184.
- (2) Güthenke, A.; Chatterjee, D.; Weibel, M.; Krutzsch, B.; Kočí, P.; Marek, M.; Nova, I.;

- Tronconi, E. Current Status of Modeling Lean Exhaust Gas Aftertreatment Catalysts. *Adv. Chem. Eng.* **2007**, *33*, 103–283.
- (3) Deutschmann, O.; Grunwaldt, J.-D. Exhaust Gas Aftertreatment in Mobile Systems: Status, Challenges, and Perspectives. *Chemie Ing. Tech.* **2013**, *85* (5), 595–617.
- (4) International Organization of Motor Vehicle. World Motor Vehicle Production By Country And Type <http://www.oica.net/wp-content/uploads/By-country-2019.pdf> (accessed Sep 28, 2020).
- (5) Buzková Arvajová, A.; Březina, J.; Pečinka, R.; Kočí, P. Modeling of Two-Step CO Oxidation Light-off on Pt/ $\gamma$ -Al<sub>2</sub>O<sub>3</sub> in the Presence of C<sub>3</sub>H<sub>6</sub> and NO<sub>x</sub>. *Appl. Catal. B Environ.* **2018**, *233*, 167–174.
- (6) Winkler, A.; Ferri, D.; Aguirre, M. The Influence of Chemical and Thermal Aging on the Catalytic Activity of a Monolithic Diesel Oxidation Catalyst. *Appl. Catal. B Environ.* **2009**, *93* (1–2), 177–184.
- (7) Ogel, E.; Casapu, M.; Doronkin, D. E.; Popescu, R.; Störmer, H.; Mechler, C.; Marzun, G.; Barcikowski, S.; Türk, M.; Grunwaldt, J.-D. Impact of Preparation Method and Hydrothermal Aging on Particle Size Distribution of Pt/ $\gamma$ -Al<sub>2</sub>O<sub>3</sub> and Its Performance in CO and NO Oxidation. *J. Phys. Chem. C* **2019**, *123* (9), 5433–5446.
- (8) Nagai, Y.; Hirabayashi, T.; Dohmae, K.; Takagi, N.; Minami, T.; Shinjoh, H.; Matsumoto, S. Sintering Inhibition Mechanism of Platinum Supported on Ceria-Based Oxide and Pt-Oxide–Support Interaction. *J. Catal.* **2006**, *242* (1), 103–109.
- (9) Jones, J.; Xiong, H.; DeLaRiva, A. T.; Peterson, E. J.; Pham, H.; Challa, S. R.; Qi, G.; Oh, S.; Wiebenga, M. H.; Pereira Hernández, X. I.; Wang, Y.; Datye, A. K. Thermally Stable Single-Atom Platinum-on-Ceria Catalysts via Atom Trapping. *Science* **2016**, *353* (6295), 150–154.

- (10) Holmgren, A.; Azarnoush, F.; Fridell, E. Influence of Pre-Treatment on the Low-Temperature Activity of Pt/Ceria. *Appl. Catal. B Environ.* **1999**, *22* (1), 49–61.
- (11) Lott, P.; Dolcet, P.; Casapu, M.; Grunwaldt, J.-D.; Deutschmann, O. The Effect of Prereduction on the Performance of Pd/Al<sub>2</sub>O<sub>3</sub> and Pd/CeO<sub>2</sub> Catalysts during Methane Oxidation. *Ind. Eng. Chem. Res.* **2019**, *58* (28), 12561–12570.
- (12) Gänzler, A. M.; Casapu, M.; Vernoux, P.; Loridant, S.; Cadete Santos Aires, F. J.; Epicier, T.; Betz, B.; Hoyer, R.; Grunwaldt, J.-D. Tuning the Structure of Platinum Particles on Ceria In Situ for Enhancing the Catalytic Performance of Exhaust Gas Catalysts. *Angew. Chemie Int. Ed.* **2017**, *56* (42), 13078–13082.
- (13) Gänzler, A. M.; Casapu, M.; Maurer, F.; Störmer, H.; Gerthsen, D.; Ferré, G.; Vernoux, P.; Bornmann, B.; Frahm, R.; Murzin, V.; Nachtegaal, M.; Votsmeier, M.; Grunwaldt, J.-D. Tuning the Pt/CeO<sub>2</sub> Interface by in Situ Variation of the Pt Particle Size. *ACS Catal.* **2018**, *8* (6), 4800–4811.
- (14) Boubnov, A.; Dahl, S.; Johnson, E.; Molina, A. P.; Simonsen, S. B.; Cano, F. M.; Helveg, S.; Lemus-Yegres, L. J.; Grunwaldt, J.-D. Structure-Activity Relationships of Pt/Al<sub>2</sub>O<sub>3</sub> Catalysts for CO and NO Oxidation at Diesel Exhaust Conditions. *Appl. Catal. B Environ.* **2012**, *126*, 315–325.
- (15) Casapu, M.; Fischer, A.; Gänzler, A. M.; Popescu, R.; Crone, M.; Gerthsen, D.; Türk, M.; Grunwaldt, J.-D. Origin of the Normal and Inverse Hysteresis Behavior during CO Oxidation over Pt/Al<sub>2</sub>O<sub>3</sub>. *ACS Catal.* **2017**, *7* (1), 343–355.
- (16) Yang, M.; Flytzani-Stephanopoulos, M. Design of Single-Atom Metal Catalysts on Various Supports for the Low-Temperature Water-Gas Shift Reaction. *Catal. Today* **2017**, *298*, 216–225.
- (17) Ammal, S. C.; Heyden, A. Understanding the Nature and Activity of Supported Platinum

- Catalysts for the Water-Gas Shift Reaction: From Metallic Nanoclusters to Alkali-Stabilized Single-Atom Cations. *ACS Catal.* **2019**, *9* (9), 7721–7740.
- (18) Maurer, F.; Jelic, J.; Wang, J.; Gänzler, A.; Dolcet, P.; Wöll, C.; Wang, Y.; Studt, F.; Casapu, M.; Grunwaldt, J.-D. Tracking the Formation, Fate and Consequence for Catalytic Activity of Pt Single Sites on CeO<sub>2</sub>. *Nat. Catal.* **2020**, *3* (10), 824–833.
- (19) Weiss, B. M.; Iglesia, E. NO Oxidation Catalysis on Pt Clusters: Elementary Steps, Structural Requirements, and Synergistic Effects of NO<sub>2</sub> Adsorption Sites. *J. Phys. Chem. C* **2009**, *113* (30), 13331–13340.
- (20) Yoon, S.; Kim, H.; Kim, D.; Park, S. Effect of the Fuel Injection Strategy on Diesel Particulate Filter Regeneration in a Single-Cylinder Diesel Engine. *J. Eng. Gas Turbines Power* **2016**, *138* (10), 102810.
- (21) James, D.; Fourré, E.; Ishii, M.; Bowker, M. Catalytic Decomposition/Regeneration of Pt/Ba(NO<sub>3</sub>)<sub>2</sub> Catalysts: NO<sub>x</sub> Storage and Reduction. *Appl. Catal. B Environ.* **2003**, *45* (2), 147–159.
- (22) Reihani, A.; Fisher, G. B.; Hoard, J. W.; Theis, J. R.; Pakko, J. D.; Lambert, C. K. Rapidly Pulsed Reductants for Diesel NO<sub>x</sub> Reduction with Lean NO<sub>x</sub> Traps: Effects of Pulsing Parameters on Performance. *Appl. Catal. B Environ.* **2018**, *223*, 177–191.
- (23) Betz, B. Low Temperature CO Oxidation on Pt/CeO<sub>2</sub> Containing Catalysts, Technical University of Darmstadt, Darmstadt, Germany, 2019.
- (24) Datye, A. K.; Votsmeier, M. Opportunities and Challenges in the Development of Advanced Materials for Emission Control Catalysts. *Nat. Mater.* 2020. <https://doi.org/10.1038/s41563-020-00805-3>
- (25) Northrop, W. F.; Jacobs, T. J.; Assanis, D. N.; Bohac, S. V. Deactivation of a Diesel Oxidation Catalyst Due to Exhaust Species from Rich Premixed Compression Ignition

- Combustion in a Light-Duty Diesel Engine. *Int. J. Engine Res.* **2007**, *8* (6), 487–498.
- (26) Steinbrüchel, C.; Schmidt, L. D. Heat Dissipation in Catalytic Reactions on Supported Crystallites. *Surf. Sci.* **1973**, *40* (3), 693–707.
- (27) Kipnis, M. Gold in CO Oxidation and PROX: The Role of Reaction Exothermicity and Nanometer-Scale Particle Size. *Appl. Catal. B, Environ.* **2014**, *152–153*, 38–45.
- (28) Gänzler, A. M.; Casapu, M.; Boubnov, A.; Müller, O.; Conrad, S.; Lichtenberg, H.; Frahm, R.; Grunwaldt, J.-D. Operando Spatially and Time-Resolved X-Ray Absorption Spectroscopy and Infrared Thermography during Oscillatory CO Oxidation. *J. Catal.* **2015**, *328*, 216–224.
- (29) Soubaihi, R. M. Al; Saoud, K. M.; Dutta, J. Critical Review of Low-Temperature CO Oxidation and Hysteresis Phenomenon on Heterogeneous Catalysts. *Catalysts* **2018**, *8* (12), 660.
- (30) Donazzi, A.; Livio, D.; Maestri, M.; Beretta, A.; Groppi, G.; Tronconi, E.; Forzatti, P. Synergy of Homogeneous and Heterogeneous Chemistry Probed by In Situ Spatially Resolved Measurements of Temperature and Composition. *Angew. Chemie* **2011**, *123* (17), 4029–4032.
- (31) Donazzi, A.; Maestri, M.; Michael, B. C.; Beretta, A.; Forzatti, P.; Groppi, G.; Tronconi, E.; Schmidt, L. D.; Vlachos, D. G. Microkinetic Modeling of Spatially Resolved Autothermal CH<sub>4</sub> Catalytic Partial Oxidation Experiments over Rh-Coated Foams. *J. Catal.* **2010**, *275* (2), 270–279.
- (32) Newton, M. A. Time Resolved Operando X-Ray Techniques in Catalysis, a Case Study: CO Oxidation by O<sub>2</sub> over Pt Surfaces and Alumina Supported Pt Catalysts. *Catalysts* **2017**, *7* (2), 58.
- (33) Dann, E. K.; Gibson, E. K.; Catlow, C. R. A.; Celorrio, V.; Collier, P.; Eralp, T.; Amboage,



- M.; Hardacre, C.; Stere, C.; Kroner, A.; Raj, A.; Rogers, S.; Goguet, A.; Wells, P. P. Combined Spatially Resolved Operando Spectroscopy: New Insights into Kinetic Oscillations of CO Oxidation on Pd/ $\gamma$ -Al<sub>2</sub>O<sub>3</sub>. *J. Catal.* **2019**, *373*, 201–208.
- (34) Hannemann, S.; Grunwaldt, J.-D.; van Vegten, N.; Baiker, A.; Boye, P.; Schroer, C. G. Distinct Spatial Changes of the Catalyst Structure inside a Fixed-Bed Microreactor during the Partial Oxidation of Methane over Rh/Al<sub>2</sub>O<sub>3</sub>. *Catal. Today* **2007**, *126* (1–2), 54–63.
- (35) Grunwaldt, J.-D.; Hannemann, S.; Schroer, C. G.; Baiker, A. 2D-Mapping of the Catalyst Structure inside a Catalytic Microreactor at Work: Partial Oxidation of Methane over Rh/Al<sub>2</sub>O<sub>3</sub>. *J. Phys. Chem. B* **2006**, *110* (17), 8674–8680.
- (36) Stötzel, J.; Frahm, R.; Kimmerle, B.; Nachtegaal, M.; Grunwaldt, J.-D. Oscillatory Behavior during the Catalytic Partial Oxidation of Methane: Following Dynamic Structural Changes of Palladium Using the QEXAFS Technique. *J. Phys. Chem. C* **2012**, *116* (1), 599–609.
- (37) Gänzler, A. M.; Casapu, M.; Boubnov, A.; Müller, O.; Conrad, S.; Lichtenberg, H.; Frahm, R.; Grunwaldt, J.-D. Operando Spatially and Time-Resolved X-Ray Absorption Spectroscopy and Infrared Thermography during Oscillatory CO Oxidation. *J. Catal.* **2015**, *328*, 216–224.
- (38) Urakawa, A.; Maeda, N.; Baiker, A. Space- and Time-Resolved Combined DRIFT and Raman Spectroscopy: Monitoring Dynamic Surface and Bulk Processes during NO<sub>x</sub> Storage Reduction. *Angew. Chemie Int. Ed.* **2008**, *47* (48), 9256–9259.
- (39) Diehm, C.; Deutschmann, O. Hydrogen Production by Catalytic Partial Oxidation of Methane over Staged Pd/Rh Coated Monoliths: Spatially Resolved Concentration and Temperature Profiles. *Int. J. Hydrogen Energy* **2014**, *39* (31), 17998–18004.
- (40) Gänzler, A. M.; Casapu, M.; Doronkin, D. E.; Maurer, F.; Lott, P.; Glatzel, P.; Votsmeier, M.; Deutschmann, O.; Grunwaldt, J.-D. Unravelling the Different Reaction Pathways for

- Low Temperature CO Oxidation on Pt/CeO<sub>2</sub> and Pt/Al<sub>2</sub>O<sub>3</sub> by Spatially Resolved Structure–Activity Correlations. *J. Phys. Chem. Lett.* **2019**, *10* (24), 7698–7705.
- (41) Nagai, Y.; Kato, A.; Iwasaki, M.; Kishita, K. Mechanistic Insights into a NO<sub>x</sub> Storage-Reduction (NSR) Catalyst by Spatiotemporal Operando X-Ray Absorption Spectroscopy. *Catal. Sci. Technol.* **2019**, *9* (5), 1103–1107.
- (42) Becher, J.; Sanchez, D. F.; Doronkin, D. E.; Zengel, D.; Meira, D. M.; Pascarelli, S.; Grunwaldt, J.-D.; Sheppard, T. L. Chemical Gradients in Automotive Cu-SSZ-13 Catalysts for NO<sub>x</sub> Removal Revealed by Operando X-Ray Spectrotomography. *Nat. Catal.* **2021**, *4* (1), 46–53.
- (43) Bornmann, B.; Kläs, J.; Müller, O.; Lützenkirchen-Hecht, D.; Frahm, R. The Quick EXAFS Setup at Beamline P64 at PETRA III for up to 200 Spectra per Second. *AIP Conf. Proc.* **2019**, *2054* (1), 040008.
- (44) Topsøe, H. Developments in Operando Studies and in Situ Characterization of Heterogeneous Catalysts. *J. Catal.* **2003**, *216* (1–2), 155–164.
- (45) Grunwaldt, J.-D.; Caravati, M.; Hannemann, S.; Baiker, A. X-Ray Absorption Spectroscopy under Reaction Conditions: Suitability of Different Reaction Cells for Combined Catalyst Characterization and Time-Resolved Studies. *Phys. Chem. Chem. Phys.* **2004**, *6* (11), 3037.
- (46) Müller, O.; Stötzel, J.; Lützenkirchen-Hecht, D.; Frahm, R. Gridded Ionization Chambers for Time Resolved X-Ray Absorption Spectroscopy. *J. Phys. Conf. Ser.* **2013**, *425* (9), 092010.
- (47) JAQ - JAQ Analyzes QEXAFS 3.3 Download <https://jaq-jaq-analyzes-qexafs.software.informer.com/3.3/> (accessed Oct 19, 2020).
- (48) Ravel, B.; Newville, M.; IUCr. *ATHENA*, *ARTEMIS*, *HEPHAESTUS*: Data Analysis for X-Ray Absorption Spectroscopy Using *IFEFFIT*. *J. Synchrotron Radiat.* **2005**, *12* (4), 537–

- 541.
- (49) Newville, M. Larch: An Analysis Package for XAFS and Related Spectroscopies. *J. Phys. Conf. Ser.* **2013**, 430 (1), 012007.
- (50) InfraTec GmbH Infrarotsensorik und Messtechnik. *Softwarefamilie IRBIS® 3 Spezialsoftware Zur Komfortablen Kamerasteuerung Und Analyse von Thermografieaufnahmen Zahlreiche Analysefunktionen Und-Werkzeuge Umfangreiche Visuelle Darstellungen Der Messdaten Professionelle Erstellung von Thermografieberichte*; 2020.
- (51) Karinshak, K. A.; Lott, P.; Harold, M. P.; Deutschmann, O. *In Situ* Activation of Bimetallic Pd–Pt Methane Oxidation Catalysts. *ChemCatChem* **2020**, 12 (14), 3712–3720.
- (52) Nguyen, H.; Harold, M. P.; Luss, D. Spatiotemporal Behavior of Pt/Rh/CeO<sub>2</sub>/BaO Catalyst during Lean-Rich Cycling. *Chem. Eng. J.* **2015**, 262, 464–477.
- (53) Gänzler, A. M.; Betz, B.; Baier-Stegmaier, S.; Belin, S.; Briois, V.; Votsmeier, M.; Casapu, M. Operando X-Ray Absorption Spectroscopy Study During Conditioning of Pt-Based Catalysts and Its Implications for CO Oxidation. *J. Phys. Chem. C* **2020**, 124 (37), 20090–20100.
- (54) Casapu, M.; Fischer, A.; Gänzler, A. M.; Popescu, R.; Crone, M.; Gerthsen, D.; Türk, M.; Grunwaldt, J.-D. Origin of the Normal and Inverse Hysteresis Behavior during CO Oxidation over Pt/Al<sub>2</sub>O<sub>3</sub>. *ACS Catal.* **2017**, 7 (1), 343–355.
- (55) Ting, A. W. L.; Balakotaiah, V.; Harold, M. P. Fast Cycling NO<sub>x</sub> Storage and Reduction: Modeling and Analysis of Reaction Pathways, Transport and Reductant Effects. *Chem. Eng. J.* **2019**, 370, 1493–1510.
- (56) Eigenberger, G.; Ruppel, W. Catalytic Fixed-Bed Reactors. In *Ullmann's Encyclopedia of Industrial Chemistry*; Wiley-VCH Verlag GmbH & Co. KGaA: Weinheim, Germany, 2012.

- (57) de Graaf, J.; van Dillen, A. J.; de Jong, K. P.; Koningsberger, D. C. Preparation of Highly Dispersed Pt Particles in Zeolite Y with a Narrow Particle Size Distribution: Characterization by Hydrogen Chemisorption, TEM, EXAFS Spectroscopy, and Particle Modeling. *J. Catal.* **2001**, *203* (2), 307–321.
- (58) Beretta, A.; Donazzi, A.; Livio, D.; Maestri, M.; Groppi, G.; Tronconi, E.; Forzatti, P. Optimal Design of a CH<sub>4</sub> CPO-Reformer with Honeycomb Catalyst: Combined Effect of Catalyst Load and Channel Size on the Surface Temperature Profile. *Catal. Today* **2011**, *171* (1), 79–83.